HHS Public Access

Author manuscript

Nature. Author manuscript; available in PMC 2017 November 04.

Published in final edited form as:

Nature. 2016 November 10; 539(7628): 294–298. doi:10.1038/nature20117.

Fatty acid synthesis configures the plasma membrane for inflammation in diabetes

Xiaochao Wei[1], **Haowei Song**[1], **Li Yin**[1], **Michael G. Rizzo Jr.**[1], **Rohini Sidhu**[2], **Douglas F. Covey**[3], **Daniel S. Ory**[2], and **Clay F. Semenkovich**[1,4]

[1]Division of Endocrinology, Metabolism & Lipid Research, Washington University School of Medicine, St. Louis, Missouri, USA

[2]Diabetic Cardiovascular Disease Center, Washington University School of Medicine, St. Louis, Missouri, USA

[3]Department of Developmental Biology, Washington University School of Medicine, St. Louis, Missouri, USA

[4]Department of Cell Biology & Physiology, Washington University School of Medicine, St. Louis, Missouri, USA

Abstract

Dietary fat promotes pathological insulin resistance through chronic inflammation[1–3]. Macrophage inactivation of inflammatory proteins improves diet-induced diabetes[4], but how nutrient-dense diets induce diabetes is unknown[5]. Membrane lipids affect the innate immune response[6], which requires domains[7] that influence high-fat diet (HFD)-induced chronic inflammation[8,9] and alter cell function based on phospholipid composition[10]. Endogenous fatty acid synthesis, mediated by fatty acid synthase (FAS)[11], affects membrane composition. Here we show that macrophage FAS is indispensable for dietinduced inflammation. Deleting FAS in macrophages prevents diet-induced insulin resistance, adipose macrophage recruitment, and chronic inflammation in mice. FAS deficiency alters membrane order and composition, impairing retention of plasma membrane cholesterol, as well as disrupting Rho GTPase trafficking required for cell adhesion, migration, and activation. Expressing a constitutively active Rho GTPase restored inflammatory signaling. Exogenous palmitate partitioned to different pools than endogenous lipids and did not rescue inflammatory signaling. However, exogenous cholesterol as well as other planar sterols rescued signaling, and exogenous cholesterol restored FAS-induced perturbations in membrane order. Endogenous fat production in macrophages is necessary for exogenous fat-induced insulin resistance by creating a receptive environment at the plasma membrane for assembly of cholesterol-dependent signaling networks.

Correspondence and requests for materials should be addressed to C.F.S. (csemenko@wustl.edu).

Author Contributions: X.W., H.S., L.Y., M.R., and R.S. performed the experiments. H.S. performed lipidomic and proteomic analyses. R.S. and D.S.O. designed and performed the analysis for oxysterols. D.F.C. designed experiments using sterol analogs. X.W. and C.F.S. designed the experiments, analyzed all data, and wrote the manuscript.

The authors declare no competing financial interests.

LysM-FAS mice (with LysM-Cre-induced myeloid cell FAS deficiency) have normal glucose tolerance on chow, but improved glucose tolerance on a HFD, lower glucose in response to insulin, and lower insulin levels as compared to controls, despite no differences in body composition or weight (Fig. 1a–d). Insulin-stimulated phosphorylation of Akt was increased in adipose and liver of LysM-FAS mice (Fig. 1e, f), indicating insulin sensitivity. There were fewer crown-like structures (Fig. 1g, h) and total (Fig. 1i) as well as pro-inflammatory (Extended Data Fig. 1a) macrophages in the visceral fat of LysM-FAS mice. As compared to controls, inflammatory gene expression (Fig. 1j) and phosphorylated c-Jun N-terminal Kinase (JNK) (Fig. 1k), which promotes obesity-associated insulin resistance, were decreased in adipose tissue of HFD-fed LysM-FAS mice. Steatosis (Fig. 1l–n) and inflammatory gene expression (Fig. 1o) were decreased in livers of HFD-fed LysM-FAS mice. These results suggest that macrophage FAS promotes diet-induced insulin resistance.

FAS protein increased when murine bone marrow-derived macrophages from control mice or RAW 264.7 macrophage-like cells were exposed to high dose palmitate or lipopolysaccharide (LPS) (Extended Data Fig. 1b–e), indicating that endogenous fatty acid synthesis is associated with macrophage activation. In response to LPS (Fig. 2a, b) or palmitate (Fig. 2c, d), peritoneal macrophages from LysM-FAS mice had decreased phospho-JNK and inflammatory cytokine generation compared to controls. Pharmacologic inhibition of FAS enzyme activity decreased LPS-induced JNK phosphorylation (Extended Data Fig. 1f). FAS knockdown in RAW 264.7 cells decreased JNK phosphorylation and inflammatory cytokine generation (Extended Data Fig. 1g–k).

Tie2-FAS mice (with Tie2-Cre-induced endothelial and hematopoietic cell FAS deficiency) have defective angiogenesis but normal glucose on a chow diet[12]. Tie2-FAS mice and wild type mice infused with bone marrow from Tie2-FAS mice as compared to respective controls were protected from diet-induced insulin resistance and inflammation (Extended Data Fig. 2–4). Thus FAS deficiency, in different Cre mice and with genetic and chemical approaches in cultured cells, decreases macrophage activation.

^{14}C-acetate incubation of macrophages demonstrated distinct effects of inhibiting fatty acid and cholesterol synthesis on whole cell accumulation of labeled lipids (Fig. 2e) with effects mostly reflected in labile detergent-resistant microdomains (DRMs) (Fig. 2f), suggesting that FAS-dependent lipids and newly synthesized sterols are channeled to DRMs. DRM-associated glycerophospholipids were decreased in FAS-deficient macrophages but there was minimal effect in whole cell membranes (Extended Data Fig. 5), suggesting that FAS deficiency alters microdomain phospholipids while preserving whole membrane lipid composition. Proteomic analysis[13] of DRMs from FAS replete (control) and FAS-deficient (from LysM-Cre and Tie2-Cre models) macrophages (Extended Data Fig. 6a with signals presented as % of control in Extended Data Fig. 6b, Supplementary Table 1) showed that 534 of 794 proteins were reduced >40% in DRMs with FAS deficiency. In whole membranes, only 17 of 681 proteins were reduced >40% with FAS deficiency (Extended Data Fig. 6c with signals presented as % of control in Extended Data Fig. 6d, Supplementary Table 2). LysM-FAS and Tie2-FAS models showed coordinate suppression of the same proteins in DRMs and little effect on whole membrane protein content (Extended Data Fig. 6e). FAS affected proteins involved in phagocytosis (Extended Data

Fig. 6f top) and responses to pathogens (Extended Data Fig. 6f middle), functions known to be DRM-dependent[14]. Proteins mediating macrophage inflammation also appeared to require FAS for DRM localization (Extended Data Fig. 6f bottom in red and Extended Data Fig. 6g). In both FAS deficiency models (Extended Data Fig. 6h), nearly all of these proteins showed decreased abundance in DRMs but not in whole membranes, results confirmed by Western blots (Extended Data Fig. 6i) including control proteins unaffected by the lack of FAS such as the archetypal non-DRM protein transferrin receptor (TfR) as well as the DRM proteins flotillin-1 and Lyn.

Cdc42, Rac, moesin, RhoA, myosin, and actin, which require dynamic trafficking through DRMs[14–20], were decreased in FAS-deficient DRMs (Extended Data Fig. 6i). Activities of Rho family GTPases were reduced in adipose tissue of LysM-FAS (Fig. 3a) and Tie2-FAS BMT (Extended Data Fig. 7a) mice fed HFD, as well as FAS-deficient macrophages (Fig. 3b) and RAW 264.7 cells (Extended Data Fig. 7b). Rho GTPases affect cell motility. Cell adhesion and migration were decreased in LysM-FAS macrophages (Extended Data Fig. 7c–e) and FAS-knockdown RAW 264.7 cells (Extended Data Fig. 7f–h) compared to controls. These findings suggest that FAS is required for macrophage inflammatory signaling by maintaining a lipid environment conducive to DRM protein trafficking.

Since DRM isolation can induce artifacts, we studied giant plasma membrane vesicles (GPMVs)21, structures at thermodynamic equilibrium. Miscibility transition temperature (at which 50% of GPMVs are phase separated as detected using the liquid disordered domain dye diI) was increased in GPMVs from LysM-FAS as compared to control macrophages (Fig. 3c), indicating an FAS-dependent difference in the separation of liquid disordered and liquid ordered domains. An increase in the difference between membrane order for distinct phases (as determined using dyes with packing-dependent emission) correlates with increased miscibility transition temperature[22]. Using the phase sensitive dye Di-4-ANEPPDHQ, the difference in general polarization (GP) was greater in LysM-FAS as compared to control GPMVs (Fig. 3d), confirming altered membrane order with FAS deficiency. When LysM-FAS and control cells were transfected with EGFP-tagged Rac followed by GPMV preparation, the Rac GFP signal was present in the liquid disordered domain (Ld) but decreased in the liquid ordered domain (Lo) with FAS deficiency (Fig. 3e–g). Rac GFP partitioning to the Lo domain was also diminished when GPMVs were prepared from FAS-deficient RAW 264.7 cells (Extended Data Fig. 8a, b). These results suggest that FAS deficiency alters membrane composition to interfere with inflammatory signaling by limiting assembly of signaling domains containing Rho GTPases. Transfection of FAS-deficient cells with a constitutively active Rac (Rac CA) under conditions that did not increase total Rac content restored JNK activation by LPS in intact LysM-FAS cells (Fig. 3h). These results confirm that FAS-deficient cells retain the capacity to transmit inflammatory signals, and suggest that FAS is important for configuring membrane composition to facilitate recruitment of signaling molecules.

In pulse labeling experiments, endogenous lipids (acetate-labeled fatty acids and cholesterol) were rapidly chased from DRMs (Fig. 4a left) but exogenous labeled palmitate accumulated in DRMs (Fig. 4a right). These results confirm that exogenous palmitate may accumulate in DRMs[9], but also indicate that endogenous and exogenous lipids access different pools. Since

DRMs require endogenous lipids, exogenous palmitate should not rescue the FAS-deficient phenotype. Pretreatment with 50 μM palmitate did not restore the JNK response to LPS (Fig. 4b) or high dose (500 μM) palmitate (Extended Data Fig. 9a). Chronic exogenous 50 μM palmitate did not normalize DRM Rho GTPase content of LysM-FAS cells and did not correct migration or adhesion defects (Extended Data Fig. 9b–d).

Cholesterol was decreased with FAS deficiency (Fig. 4c, Extended Data Fig. 9e, f). Compared to controls, cholesterol was more readily released to methyl-β-cyclodextrin by LysM-FAS cells (Fig. 4d) and FAS-deficient RAW 264.7 cells (Extended Data Fig. 9g). LysM-FAS cells had increased oxysterol synthesis in response to cholesterol loading (Fig. 4e), reflecting increased metabolism of membrane cholesterol[23], and resulting in decreased cholesterol content. Intact FAS-deficient RAW 264.7 cells had increased accessibility to cholesterol oxidase (Extended Data Fig. 9h). Thus, endogenous fatty acid synthesis in macrophages regulates intracellular cholesterol metabolism.

Loading cells with a range of cholesterol concentrations using methyl-β-cyclodextrin followed by exposure to LPS revealed differences in JNK activation (Fig. 4f). FAS-deficient cells, as expected, had decreased JNK activation compared to control cells in the absence of cholesterol loading, but low concentrations of cholesterol rescued JNK activation. When the cholesterol pulse was followed by a two-hour cholesterol-free chase before addition of LPS, JNK activation was lost (Fig. 4g). Cholesterol loading of LysM-FAS cells increased Rac content in the liquid ordered domain of GPMVs (Fig. 4h–j), and loading cells before preparing vesicles or directly adding cholesterol to vesicles corrected perturbations in membrane order (Fig. 4k). These results confirm that membrane order is cholesterol-dependent in GPMVs and correlated with DRM cholesterol content[24].

Loading macrophages with 1 μM cholesterol rescued JNK activation by LPS in LysM-FAS macrophages without significantly affecting JNK activation in controls (Fig. 4l). Loading with the enantiomer of cholesterol (*ent*-cholesterol[25]) rescued JNK activation with FAS deficiency (Fig. 4m), suggesting sterol interaction with membrane lipids rather than proteins. Loading with (3β)-26,27-dinorcholest-5-en-24-yn-3-ol, an alkyne with the cholesterol ring structure but a modified side chain, also rescued JNK activation (Fig. 4n). Loading with coprostanol, a non-planar sterol, did not (Fig. 4o). These results suggest that planar sterols (Extended Data Fig. 10a) interact with the FAS-deficient phospholipid environment to assemble signaling domains.

Endogenous synthesis of lipids in obesity-related diabetes relays physiologic cues that cannot be mimicked by chemically identical exogenous lipids, consistent with studies of lipid metabolism in viral infection[26]. FAS configures the plasma membrane to retain cholesterol required for propagating inflammatory signals, which may account for beneficial effects of FAS inhibition in animal models of diabetes[27]. Without FAS (Extended Data 10b), intrinsic phospholipids incorporate unsaturated fatty acids favoring release of cholesterol, and Rho GTPases do not activate JNK. De novo lipogenesis may also configure the lipid environment to impact dendritic cell, T helper 17 cell, and inflammasome function[28–30].

METHODS

Animal models

Hematopoietic FAS ablation mouse models LysM-FAS[31], Tie2-FAS[12], and Tie2-FAS bone marrow transplantation animals[12] were generated as described. The high fat diet was a Western-type diet containing 0.15% cholesterol with 42% calories as fat (TD 88137, Harlan). Studies were conducted with littermates in the C57BL/6 background in a specific pathogen-free facility with a 12-h light/12-h dark cycle. The local Animal Studies Committee approved experiments.

Sample sizes were based on the estimated standard deviation of previous studies in similar experimental settings. A formal randomization tool was not used to allocate animals to experimental groups. Cages containing both genotypes as littermates were selected for allocation to experimental groups. Animals were not excluded from analyses unless results could not be generated due to the death of the animal. No formal blinding was employed in the animal studies.

Metabolic phenotyping

For glucose tolerance tests, mice were injected i.p. with 1 g glucose/kg body weight after 6 h of fasting; glucose was measured in tail blood using the Contour glucometer (Bayer). Glucose-stimulated insulin secretion assays were performed in separate cohorts with insulin measured using ELISA kits (PerkinElmer). For insulin tolerance tests, mice were injected i.p. with 0.75 U insulin/kg body weight after 6 h of fasting. For insulin signaling, mice after an overnight fast were injected i.p. with 5 mU insulin/g, and tissues were collected 10 min later. Body composition analysis was determined using MRI. Liver triglycerides[32] and food intake[12] were assayed as described. Global insulin sensitivity was determined by hypersinsulinemic-euglycemic clamp as described[33]. Animals were implanted with a jugular catheter. Five days after surgery, animals were fasted for 4 h and glucose turnover was measured in the basal state and during the clamp in conscious mice.

Histology

Visceral fat was fixed in formalin. Five μm paraffin sections were stained for Mac2 (BD Bioscience) for crown-like structures. Processing included slides in the absence of primary antibody to correct for nonspecific staining. For neutral lipid detection, 10 μm frozen sections of liver were fixed with formalin (10%, Sigma) followed by Oil red O (Sigma) staining in 60% isopropanol.

Isolation of stromal-vascular cell fraction (SVF) and FACS analysis

Epididymal fat pads were isolated after saline perfusion, then minced, washed, and centrifuged (1,000 g for 5 min). Floating adipose tissue was collected and digested with type I collagenase solution (1 mg/ml, 30 min). This digest was pelleted to yield the SVF, which was washed twice in FACS wash buffer (PBS supplemented with 4% FBS), then blocked for Fc receptors using anti-mouse CD16/32 (BD Bioscience), followed by staining with APC-conjugated anti-mouse CD11b, eFluor 450- conjugated anti-mouse CD11c, and PE-conjugated anti-mouse F4/80 (eBioscience). Other surface markers included CD18 and

ICAM-1 (both PE-conjugated, eBioscience). Samples were analyzed using a BD LSD II flow cytometer.

Gene expression

Total RNA was extracted using TRIZOL (Invitrogen) and reverse transcribed using an iScript cDNA synthesis kit (Bio-Rad). PCR reactions were performed with an ABI prism 7000 sequence detection system using the SYBR Green PCR Master Mix assay and primer sequences as described[34].

Western blotting and Rho GTPase activity assays

Tissues or cultured cells were treated with lysis buffer (50 mM Tris HCl, pH 7.4, 1 mM EDTA, 150 mM NaCl, 1% NP40, 0.25% Na deoxycholate, 2 mM $NaVO_3$, 5 mM NaF, and protease inhibitors from Roche). Whole lysates or fractions were subjected to 4–20% gradient SDS-PAGE (Invitrogen) followed by immunoblotting with antibodies to FAS, transferrin receptor (Abcam), actin (Sigma), total and phospho-Akt (T308 and S473), total and phospho-JNK, Lyn, RhoA, Cdc42, Rac, moesin (Cell Signaling), flotillin-1, insulin receptor (BD Bioscience), ICAM-1, myosin (Santa Cruz), and annexin V (Biosensis). Activities of Rho family GTPases were measured by pull-down assays for GTP-bound forms of the proteins (Cytoskeleton). Lysates were mixed with PAK-GST protein beads (for GTP-Rac binding) or Rhotekin-RBD protein GST beads (for GTP-RhoA binding) and precipitates were analyzed by immunoblotting.

Cell culture and metabolic labeling

Bone marrow-derived macrophages were differentiated in DMEM plus 20% L929-conditioned media. Peritoneal macrophages were elicited by i.p. injection of 4% thioglycollate media (Sigma), and adherent cells were cultured in DMEM plus 10% FBS. RAW 264.7 cells were also cultured in DMEM plus 10% FBS. FAS was knocked down in RAW cells using a lentiviral-based shRNA strategy (Open Biosystems). 293T cells were transfected with packaging vectors along with an expression plasmid (pLKO.1-puro system) containing shRNA sequences that were scrambled or specific for mouse FAS message[34]. Two days later, viruses were collected and filtered, then used to infect RAW cells (10 μg/ml polybrene). Infected RAW cells were selected with puromycin (4 μg/ml) for 2 days.

For inflammatory activation, macrophages were treated with LPS (100 ng/ml), or high dose palmitate (500 μM/1% BSA, with BSA only as control) for 6 hours before harvest. Lysates were assayed for JNK activation by Western blotting. Supernatants were assayed for the proinflammatory cytokines TNFα, MCP1, IL1β, and IL12p40 by ELISA (R&D systems).

For lipid labeling analyses, cells were serum starved for 24 h in the absence or the presence of simvastatin (10 μM active form, Calbiochem). ^{14}C-acetate (10 μCi) was added to 10 cm culture dishes, cells were harvested after 4 h, lipids were extracted with chloroform/methanol, and radioactivity measured with a liquid scintillation counter. In chase experiments involving de novo lipid synthesis, cells were treated with ^{14}C-acetate (10 μCi) for 24 h, then chased with cold media for 0.5, 1 and 4 h. DRMs were isolated and lipid extracts were counted. In chase experiments involving palmitate, cells were incubated

with ^{14}C-palmitate (5 μCi, ~10 μM) complexed with cold palmitate (50 μM)/BSA (0.1%), then chased with cold media. In exogenous palmitate reconstitution experiments, knockout macrophages were treated with palmitate (50 μM/0.1% BSA) for 24 h with BSA only groups serving as controls.

Membrane extraction and isolation of submembrane microdomains

Cells were homogenized in hypotonic buffer (1 mM HEPES, pH 8.0, 15 mM KCl, 2 mM $MgCl_2$, 0.1 mM EDTA, and protease inhibitors from Roche). Lysates were subjected to sequential centrifugation steps (2000 g for 5 min, 10,000 g for 15 min, 100,000 g for 2 h) to yield crude membrane fractions. To isolate detergent-resistant membranes (DRMs), cells were lysed in MES buffer (10 mM MES, 150 mM NaCl, pH 6.5) containing protease inhibitors, incubated with 1% Triton X- 100 on ice for 30 min, and homogenized by 20 passes through 29-gauge needles. Homogenates were adjusted to 40% sucrose and placed under sucrose layers of 5% and 30%. After centrifugation at 39000 rpm, 4°C for 16 h, fractions were collected from top to bottom. For submembrane isolation in the absence of detergent, sodium carbonate buffer at high pH (500 mM, pH 11.0) was used and Triton X-100 was omitted in the above procedure. Sucrose layers of 5%, 35% and 45% were used to generate fractions.

Lipid analyses by electrospray ionization (ESI) MS/MS

After Bligh-Dyer extraction, organic phases were collected, dried under nitrogen, and reconstituted in 200 μl chloroform/methanol (1:1) with 0.5% sodium acetate. A 50 μl aliquot was directly injected into a Thermo Vantage triple-quadruple mass spectrometer in positive mode for the analysis of PC (including SM) species with neutral loss scan of 183, and for the analysis of PE species with neural loss scan of 141. Each individual species was compared to its internal standard, and absolute quantity was determined using a standard curve, all as described[33].

SILAC and proteomic analysis by mass spectrometry

SILAC techniques[35,36] utilized RAW 264.7 cells cultured in medium containing “heavy” ($^{13}C_6$ L-Lysine and $^{13}C_6$ L-Arginine) stable isotope labeled amino acids (Thermo Scientific). Murine bone marrow-derived macrophage cells from different genetic models were grown in “light” ($^{12}C_6$ L-Lysine and $^{12}C_6$ L-Arginine) medium. Cells were lysed, equal amounts of extracts from labeled cells were combined, then subjected to differential centrifugation for the crude membrane extraction, or sucrose gradient centrifugation for DRM extraction. Samples were resolved by SDS-PAGE, separated into 10 fractions, and in-gel trypsin digestion was performed before LC/MS/MS.

For nanoHPLC-ESI-MS/MS, studies were performed on a LTQ-Orbitrap (Thermo) instrument. Samples were loaded with an autosampler onto a 15 cm Magic C18 column (5 μm particles, 300 Å pores, Michrom Bioresources) packed into a PicoFrit tip (New Objective) and analyzed with a nanoLC-2D plus HPLC (Eksigent). Analytical gradients were from 0–80% organic phase (95% acetonitrile, 0.1% formic acid) over 60 min. Aqueous phase composition was 2% acetonitrile, 0.1% formic acid. Eluent was routed into a PV-550 nanospray ion source (New Objective). The LTQ-Orbitrap was operated in a data-dependent

mode with the precursor scan over the range *m/z* 350–2000, followed by twenty MS2 scans using parent ions selected from the MS1 scan. The Orbitrap AGC target was set to 1E06, and the MS2 AGC target was 1E04 with maximum injection times of 300 ms and 500 ms, respectively. For tandem MS, LTQ isolation width was 2 Da, normalized collision energy 30%, and activation time 10 ms.

Raw data were submitted to Mascot Server 2.0 and searched against the SwissProt database. Results were quantified by analyzing the mascot "dat" file and its respective thermo "raw" file using a locally generated program. Relative protein ratios for control versus knockout macrophages were calculated for each identified protein (averaging signal from multiple peptides) and presented as % of control in a heat map (CIMminer). Pathway analysis was performed using databases including DAVID, KEGG and PANTHER.

Analysis of giant plasma membrane vesicles (GPMVs)

GPMVs were induced in bone marrow-derived macrophages or RAW cells essentially as described[21]. Cells were rinsed with GPMV buffer (10 mM HEPES, 150 mM NaCl and 2 mM $CaCl_2$, pH 7.4) followed by 1–2 hour incubation with vesiculation-induction GPMV buffer in the presence of PFA (25 mM) and DTT (2 mM) at 37° C. The vesicles were stained using FAST-DiI (Invitrogen, 0.25 μg/ml) at room temperature for 30 min. Vesicles were imaged during temperature-controlled cooling by confocal microscopy[37]. A four-chambered coverglass containing vesicle suspensions was placed in a metal block that was gradually cooled by circulating water. Images were captured with a 20x air objective in an inverted Zeiss LSM 510 laser-scanning microscope system. An HeNe laser (at 543nm excitation) was used for FAST-DiI. In multiple scanning mode for sequential captures, an Argon laser (at 488 nm excitation) was used for EGFP imaging, and single-channel labeled cells were used to calibrate the system to exclude the leak between the two channels.

For lipid order analysis, an environmentally sensitive dye di-4-ANEPPDHQ was used as described[38]. The dye was excited by an Argon laser at 488 nm wavelength and the two-channel emission signal was collected at ~560 nm (ordered) and ~620 nm (disordered) simultaneously. Image calculations were carried out in ImageJ using GP (Generalized Polarization Analysis) plugin (http://www.optinav.com/Generalized_Polarization_Analysis.htm) with modification to include a measured G calibration factor. In order to determine the GP value, we analyzed the pictures acquired and calculated the GPs using the equation:

$$GP=\frac{I_{blue}-G\,I_{red}}{I_{blue}+G\,I_{red}}$$

where G is the calibration factor calculated using

$$G=\frac{GP_{ref}+GP_{ref}GP_{mes}-GP_{mes}-1}{GP_{mes}+GP_{ref}GP_{mes}-GP_{ref}-1}$$

GP_{mess} is the GP value of the dye in 100% DMSO measured using the same imaging settings as used for GPMVs.

For analyzing the partition patterns of Rac protein in GPMVs, cells expressing Rac-EGFP were used. A retroviral-based plasmid for EGFP conjugated wild type Rac was derived from the pMX-GFP-Rac G12V (Addgene #14567, N-terminal GFP) by site-directed mutagenesis. The plasmid was transfected into PLAT-E cells, and produced retrovirus was used to infect primary bone marrow progenitor cells during macrophage differentiation. The GPMVs generated were then labeled with FAST-DiI for monitoring phase separation, and two-channel fluorescence was captured at 15°C. The GFP fluorescence intensity peaks in the two domains were quantified. The analysis for the temperature plot of phase separation and quantitation of Rac protein membrane partition was done in ImageJ software[37].

Cell spreading and migration assays

For spreading, macrophages were plated (30,000 cells/well) into four-chambered LAB-TEK slides (Thermo Scientific). After 30 min, cells were gently washed and fixed with 4% paraformaldehyde, followed by permeabilization with 0.1% Triton X-100. The cells were then stained with rhodamine-phalloidin (Invitrogen). Cell images were captured by immunofluorescence microscopy. Individual cells were outlined, and total cell area was quantified using ImageJ software.

For migration, transwell inserts with 3 μm-pore size (Corning) were precoated with 0.2% gelatin. Macrophages were trypsinized and 20,000 cells were added in triplicate to inserts in chambers. Media with vehicle or MCP1 (100 ng/ml, R&D systems) was added to the lower wells, and 4 h later cells that had migrated to the underside of the membrane were fixed. Cells on the upper side of the membrane were removed, and membranes were cut and positioned with migrated cells facing up, followed by DAPI staining and counting.

Sterol manipulations

Cholesterol oxidase activity and membrane cholesterol release potential were measured as described[39]. Cells cultured overnight in 96-well plates were rinsed twice with PBS, then treated with 100 μl of PBS containing cholesterol oxidase (2 units/ml, Sigma) at 37°C for 10 min. Then 50 μl Amplex red reagent (Invitrogen) was added, and after incubation at 37°C for 20 min, activity was quantitated by spectrometry at 560 nm. Samples processed without cholesterol oxidase were used to determine background.

For cholesterol release potential, cells were labeled with [^{3}H] cholesterol overnight, rinsed with cold media three times then incubated with cold media containing methyl-β-cyclodextrin (1 mM, Sigma) at 37°C. Aliquots of the media were collected over time, sedimented, and the supernatants were counted. Cell lysates were also processed and counted.

For oxysterol production with cholesterol loading[23], cells were plated in 6-well plates (50,000 cells/well) and incubated overnight in medium with lipoprotein-deficient serum. Cells were treated with a methyl-β-cyclodextrin:cholesterol complex for 10 min, then washed twice and harvested for oxysterol measurements[40]. 25-hydroxycholesterol (25-HC)

and 27-hydroxycholesterol (27-HC) were extracted by the Bligh-Dyer method from homogenized macrophages and media after addition of deuterated internal standard (d5-27-HC). The organic layer was taken to dryness under nitrogen, then 50 μl of 0.5 M N,N-dimethylglycine (DMG)/2M 4-dimethylaminopyridine (DMAP) in chloroform and 50 μl of 1M 1-ethyl-3-(3-dimethylaminopropyl)carbodiimide (EDC) in chloroform were added to derivatize the samples. After incubation for 1 h at 50°C, the reaction was quenched with 50 μl of methanol. The sample was taken to dryness under nitrogen, and the residue was treated with 1:3 (v/v) water/hexane to remove the derivatizing reagent. The hexane layer was taken to dryness under nitrogen, the sample was reconstituted with 200 μl of methanol, and analyzed by LC-MS/MS using a Prominence HPLC system (Shimadzu Scientific Instruments, Columbia, MD), and a 4000QTRAP mass spectrometer (Applied Biosystems/MDS Sciex Inc., Ontario, Canada). Data were acquired using Analyst software (v.1.5.1).

Rescue of JNK signaling

To express a constitutively active form of Rac protein in FAS knockout macrophages, we used a selectable retroviral expression system using pMX-Bsd-Rac G12V. Plasmids were transfected into PLAT-E cells, and produced retrovirus was used to infect primary bone marrow progenitor cells during macrophage differentiation. On the day following infection, positive cells were selected in blasticidin (1 μ/ml). Three days later, differentiated macrophages were used for analyzing JNK response.

For cholesterol rescue experiments, different forms and concentrations of cholesterol were complexed to methyl-β-cyclodextrin (Sigma) in a ratio of 1 to 10 (with 0.25 mM cyclodextrin) and diluted to desired concentrations using serum-free media. The enantiomer of cholesterol[25] and alkyne cholesterol[41] were synthesized at Washington University. Coprostanol was purchased from Sigma. Sterol was first dried under nitrogen gas, and then sonicated into DMEM with cyclodextrin until flaky chunks disappeared. The solution was then shaken overnight at 37° C. Bone marrow-derived macrophages were pretreated by serum-free media for 2 h, and then cyclodextrin/cholesterol was added for 10 min followed by 30 min exposure to LPS (100 ng/ml). For the “cholesterol pulse” experiment, a two-hour serum-free media incubation followed cyclodextrin/cholesterol exposure before LPS was added. For reconstitution of cholesterol in GPMVs, cells were treated with cholesterol (25 μM) overnight followed by vesicle preparation. For some experiments, cholesterol solution was added directly to vesicle suspensions at 5 μg/ml.

Statistical analyses

Data are expressed as means +/− standard error of the mean (s.e.m.). Analyses were performed with Prism, by two-tailed t-test (two groups), by one way ANOVA (more than two groups) and Tukey’s multiple comparison test, by two way ANOVA (two independent variables) and Bonferroni posttests, or by nonlinear curve fit comparison. $P<0.05$ was considered significant and is indicated by * (except for results of nonlinear curve fit comparisons where * indicates $P<0.001$). For analysis of proteomic data, pathways with $P<0.05$ (modified Fisher Exact P-Value for gene-enrichment analysis) were selected for protein-protein interaction maps generated by STRING.

Extended Data

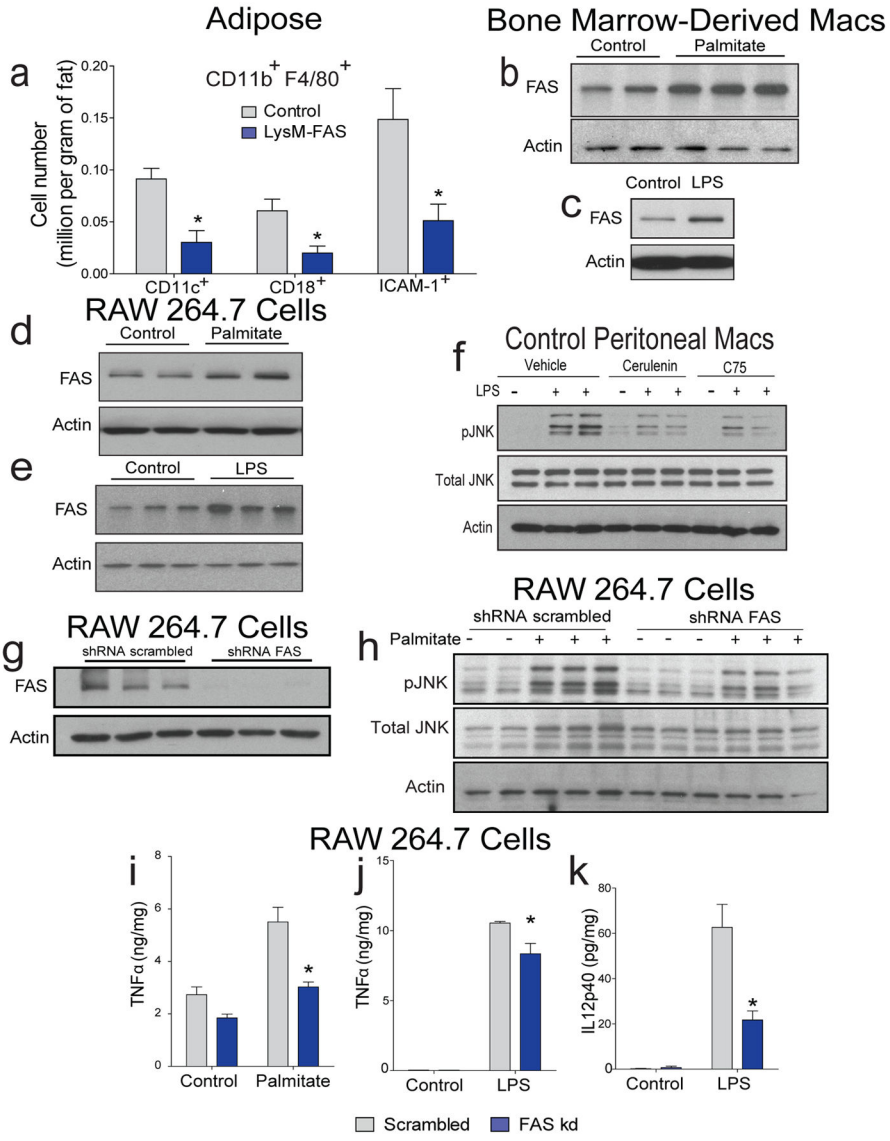

Extended Data Fig. 1. FAS is induced by inflammatory stimuli and its deficiency suppresses inflammation

a. Quantitation of subsets of pro-inflammatory macrophages (additionally positive for CD11c, CD18, or ICAM1) in the adipose tissue from HFD-fed control and LysM-FAS mice (n=4). **b, c.** Western blotting of FAS protein in bone marrow-derived macrophages treated with vehicle as control, palmitate (500 μM) or LPS (100 ng/ml). **d, e.** Western blotting of FAS protein in RAW cells treated with vehicle as control, palmitate (500 μM) or LPS (100 ng/ml). **f**. JNK phosphorylation with LPS stimulation in the presence of FAS inhibitors cerulenin or C75. **g**. Western blotting of FAS protein in RAW cells treated with scrambled control or a lentiviral-based shRNA targeting FAS. **h.** Phosphorylated JNK in RAW cells after stimulation with palmitate (500 μM). **i–k.** ELISAs for pro-inflammatory cytokines in

RAW cells stimulated with palmitate (500 μM) or LPS (100 ng/ml), n=3. *P<0.05, symbols and error bars indicate mean ± s.e.m.

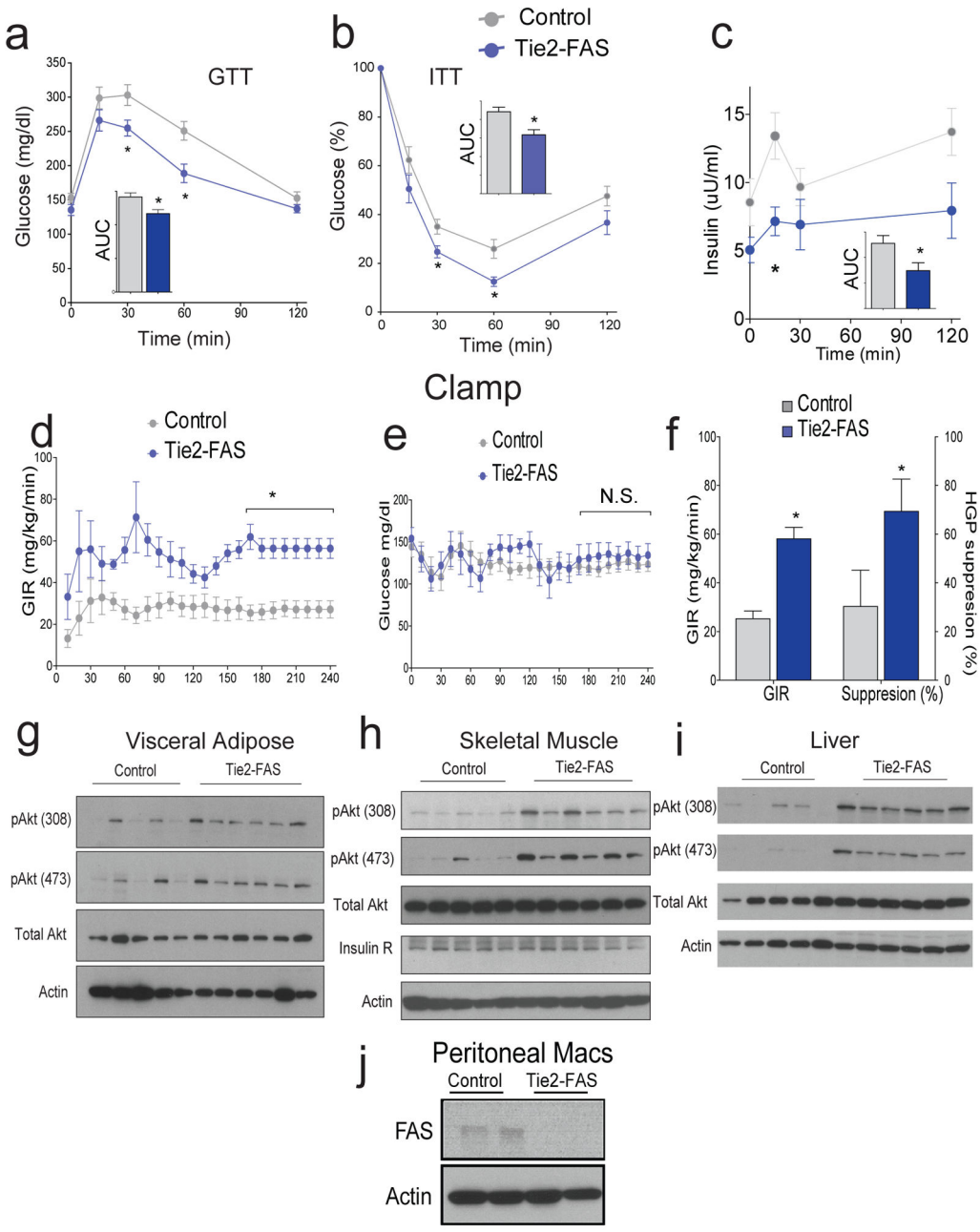

Extended Data Fig. 2. Tie2-FAS mice are protected from diet-induced insulin resistance

a. Glucose tolerance test (GTT), **(b)** insulin tolerance test (ITT), and (**c)** glucose-stimulated insulin secretion assays in control and Tie2-FAS mice fed with HFD for 3 months (n=15 control and 8 Tie2-FAS). **d**. Glucose infusion rate (GIR), and (**e**) plasma glucose levels during hyperinsulinemic-euglycemic clamping for HFD-fed control (n=9) and Tie2- FAS mice (n=6). **f**. Mean GIR and hepatic glucose production (HGP) suppression at steady state of the clamp experiment. **g–i**. Western blotting of Akt phosphorylation levels in various

mouse tissues during the clamp. **j**. Western blotting of FAS protein in peritoneal macrophages from control and Tie2-FAS mice. *P<0.05, symbols and error bars indicate mean ± s.e.m.

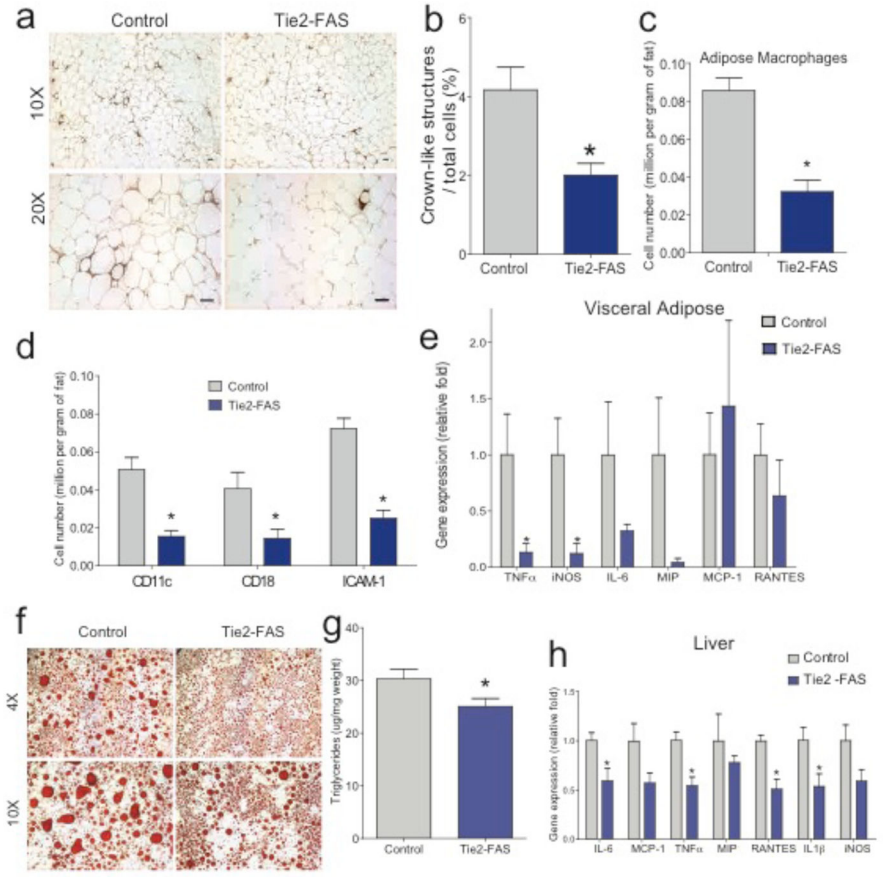

Extended Data Fig. 3. Mice with FAS deficiency induced by Tie2-Cre resist dietinduced chronic inflammation

a. Images of crown-like structures in visceral fat stained by the macrophage marker Mac2. **b**. Quantitation of crown-like structures (n=4 mice). **c, d**. Quantitation of macrophages (F4/80+ and CD11b+) and subsets of pro-inflammatory macrophages (additionally positive for CD11c, CD18 and ICAM1) in visceral adipose tissue of Tie2-FAS mice by flow cytometry (n=4 control and 5 Tie2-FAS). **e.** Gene expression in visceral adipose tissue from control (n=6) and Tie2-FAS mice (n=9). **f**. Oil red O staining of liver from Tie2-FAS mice fed HFD. **g**. Quantitation of liver fat content (n=8 control and 9 Tie2-FAS). **h**. Gene expression in liver from control (n=6) and Tie2-FAS mice (n=9). *P<0.05, symbols and error bars indicate mean ± s.e.m.

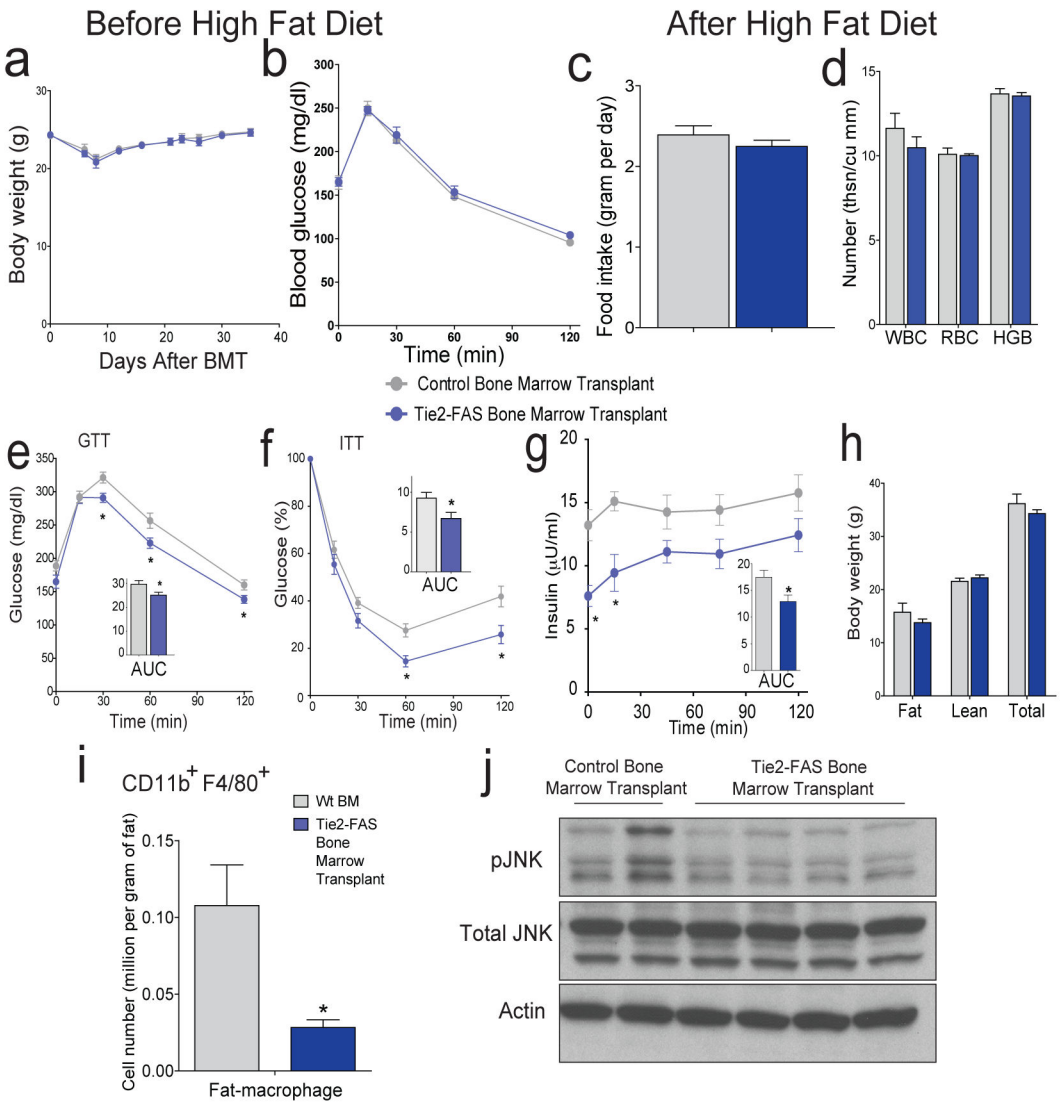

Extended Data Fig. 4. Diet effects in Tie2- FAS bone marrow transplant mice

a. Body weight measurements in mice (n=15) following bone marrow transplant with control or Tie2- FAS marrow. **b**. Glucose tolerance testing in mice (n=10) one month following bone marrow transplant (BMT) while eating chow diet. **c.** Food intake and (**d**) blood counts in mice on HFD following bone marrow transplant (n=7 control and 9 Tie2-FAS BMT). **e.** Glucose tolerance testing, (**f**) insulin tolerance testing, (**g**) glucose-stimulated insulin levels, and (**h**) body composition in control (n=17) and Tie2- FAS bone marrow transplant mice (n=15) on a high-fat diet. **i**. Inflammatory cells in visceral adipose tissue (n=4). **j**. JNK phosphorylation in adipose tissue of bone marrow transplant mice. *P<0.05, symbols and error bars indicate mean ± s.e.m.

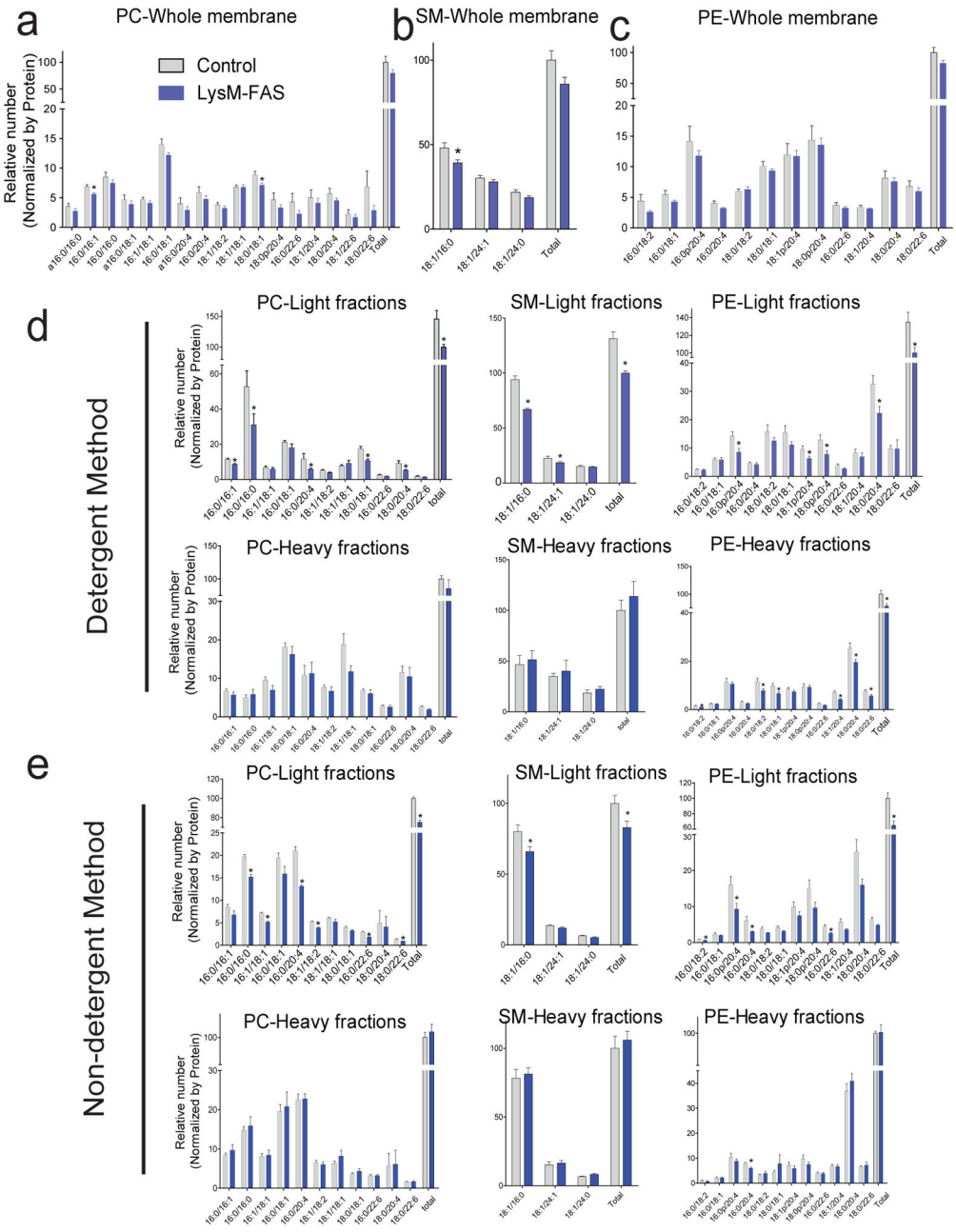

Extended Data Fig. 5. Phospholipid composition of light fractions (DRMs) and heavy fractions (non-DRM) in the presence and absence of FAS in macrophages

Mass spec quantification of phosphatidylcholine (**a**), sphingomyelin (**b**) and phosphatidylethanolamine (**c**) species of phospholipids in whole membranes (n=8). **d.** Quantification of phosphatidylcholine (PC), sphingomyelin (SM), and phosphatidylethanolamine (PE) species by the detergent method (n=7–8). (**e**) Lipid species by the non-detergent, high pH carbonate buffer method (n=4). *P<0.05, symbols and error bars indicate mean ± s.e.m.

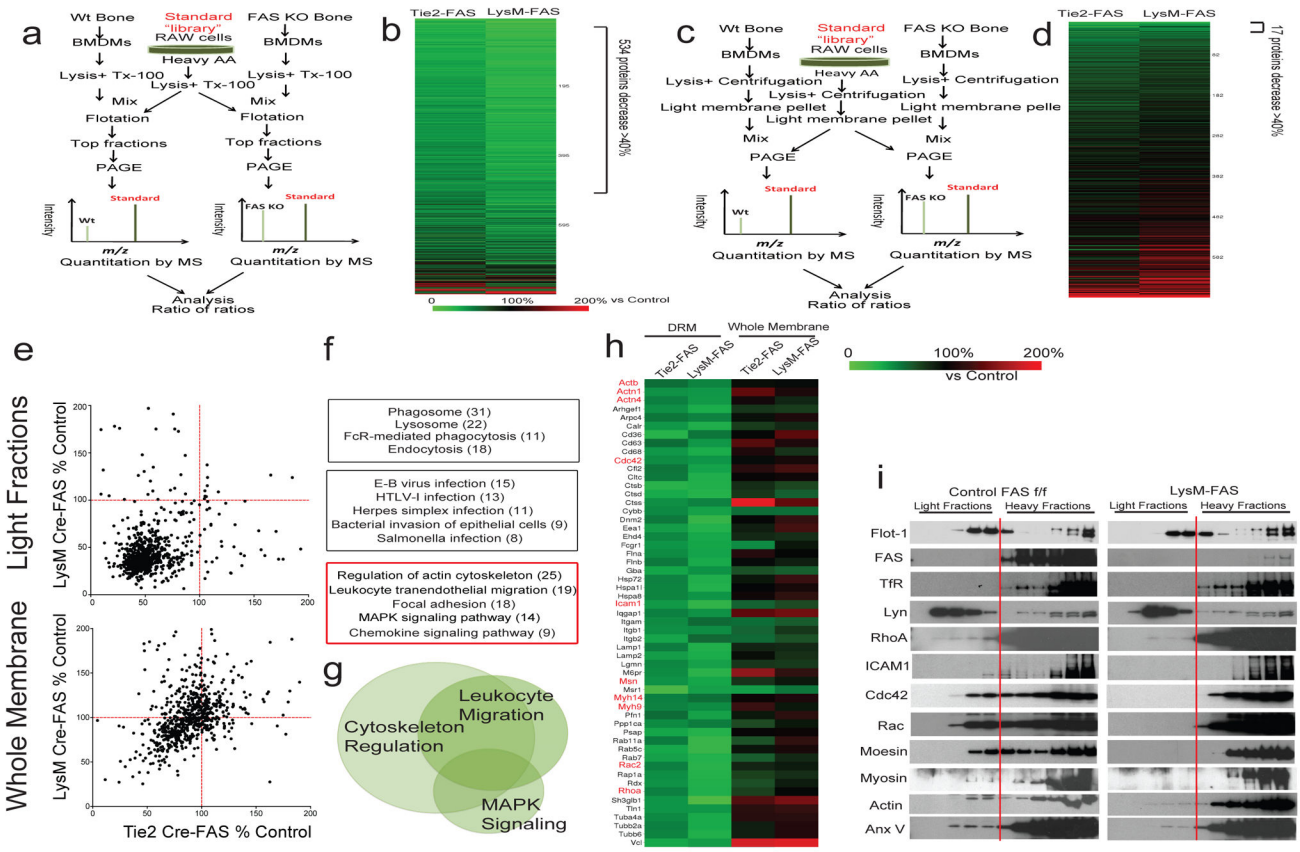

Extended Data Fig. 6. FAS is required for compartmentalizing proteins in DRMs

a. SILAC strategy for DRM proteomic analysis in bone marrow-derived macrophages (BMDMs). **b**. Heat map of relative abundance for DRM proteins in both strains (LysM-FAS and Tie2-FAS) of FAS-deficient BMDMs as compared to FAS-replete BMDMs. **c**. SILAC strategy for whole membrane proteomic analysis. **d**. Heat map of relative abundance for membrane-associated proteins in both FAS-deficient models as compared to FAS-replete cells. **e.** SILAC quantitation of DRM (top) and whole membrane (bottom) proteomes in LysM-FAS and Tie2-FAS BMDMs relative to controls. **f.** DRM proteins affected by FAS deficiency (protein numbers in parentheses) in functional classes and (**g**) pathway analysis of affected proteins in macrophage inflammation. **h.** Heat map of select proteins from **e. i**. Western blotting to confirm heat map changes of proteins indicated in red from **h**.

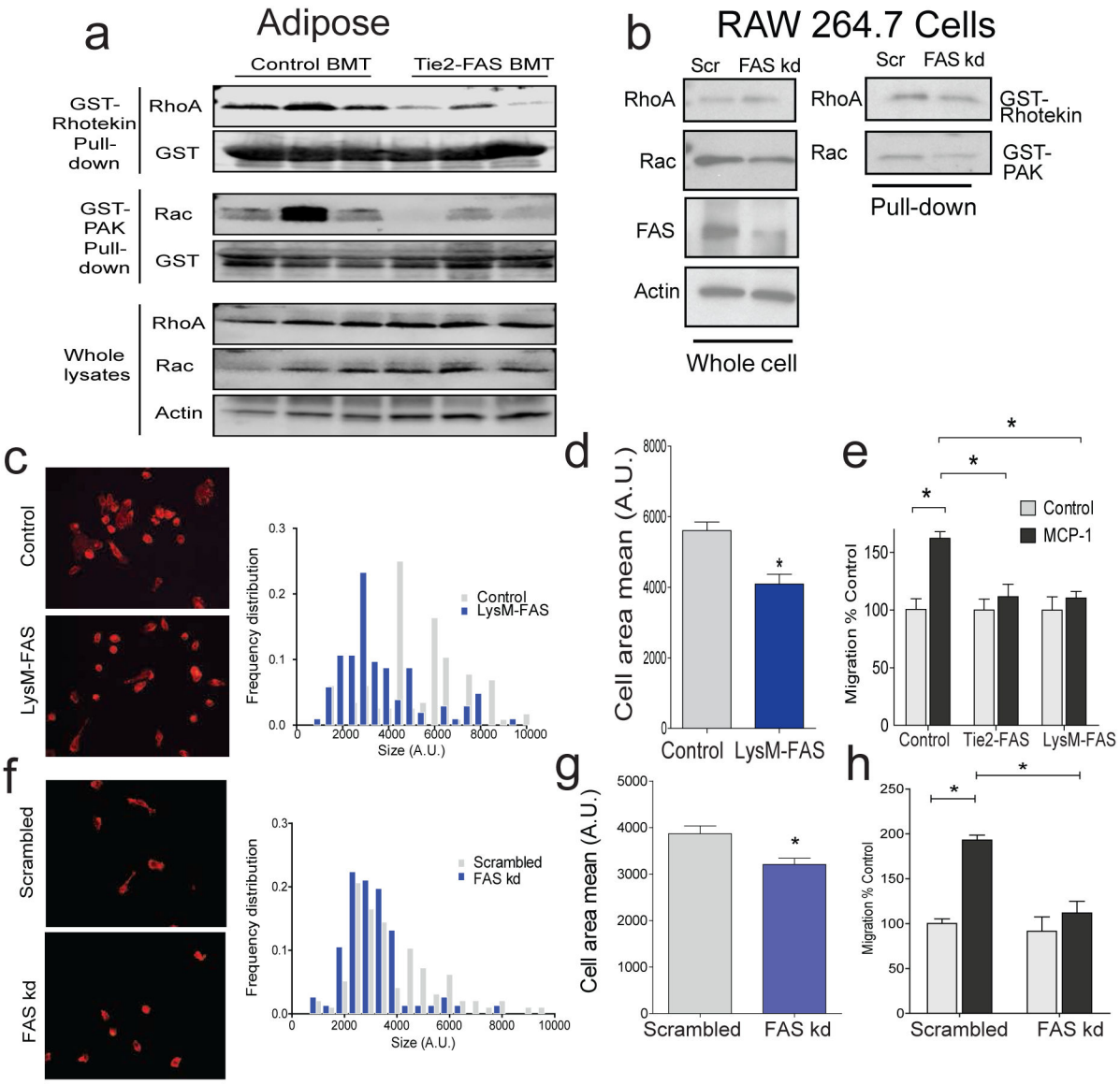

Extended Data Fig. 7. Rho family GTPase activity and cell phenotyping in the setting of FAS deficiency

a. Western blotting of activated RhoA (top panel), activated Rac (middle panel), and total RhoA and Rac (bottom panel) in adipose tissue of control and Tie2-FAS BMT mice. **b**. Western blotting of whole cells (left), or activated (right with substrate pull-down) Rho GTPases in scrambled (control) or FAS-knockdown RAW cells. **c**. Cell spreading images of FAS replete (control) and FAS deficient (LysM-FAS) bone marrow-derived macrophages with frequency distribution of cell spreading in control or FAS-deficient macrophages. **d**. Cell area for control and LysM-FAS cells. **e**. MCP1-induced transwell migration of Tie2-FAS and LysM-FAS cells (n=4). **f**. Cell spreading images of scrambled (control) and FAS deficient (FAS kd) RAW cells with frequency distribution of cell spreading in control or FAS-knockdown RAW cells. **g**. Cell area for control and FAS knockdown RAW cells. **h**. MCP1-induced transwell migration of FAS knockdown RAW cells (n=4). n>100 for

frequency distributions of cell spreading. *P<0.05, symbols and error bars indicate mean ± s.e.m.

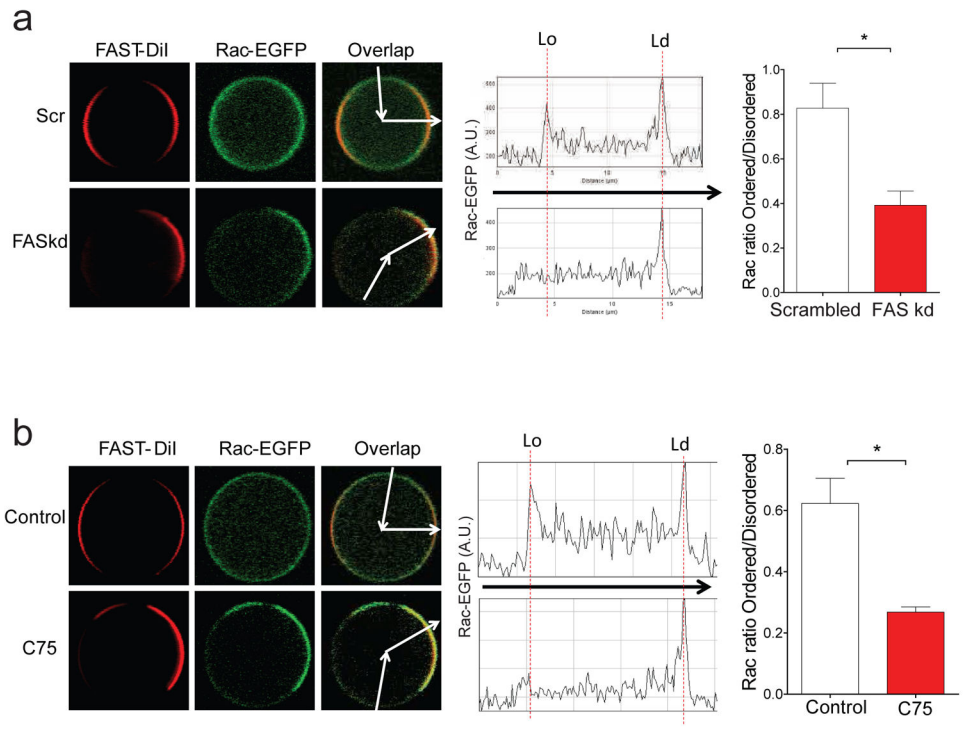

Extended Data Fig. 8. Disruption of Rho GTPase membrane localization with genetic and pharmacologic inhibition of FAS

RAW cells were transfected with a Rac-EGFP construct then subjected to FAS knockdown (**a**) or incubated with the nonspecific FAS inhibitor C75 (**b**) followed by preparation of GPMVs and phase imaging. Lo and Ld domains for quantification are indicated by arrows, an ImageJ scan of these domains is shown in the middle, and quantification of Rac partitioning in ordered vs. disordered domains is shown on the right. Imaging analyses were repeated in 3 independent experiments, and data shown are from representative experiments with 6 vesicles per group. *P<0.05, symbols and error bars indicate mean ± s.e.m.

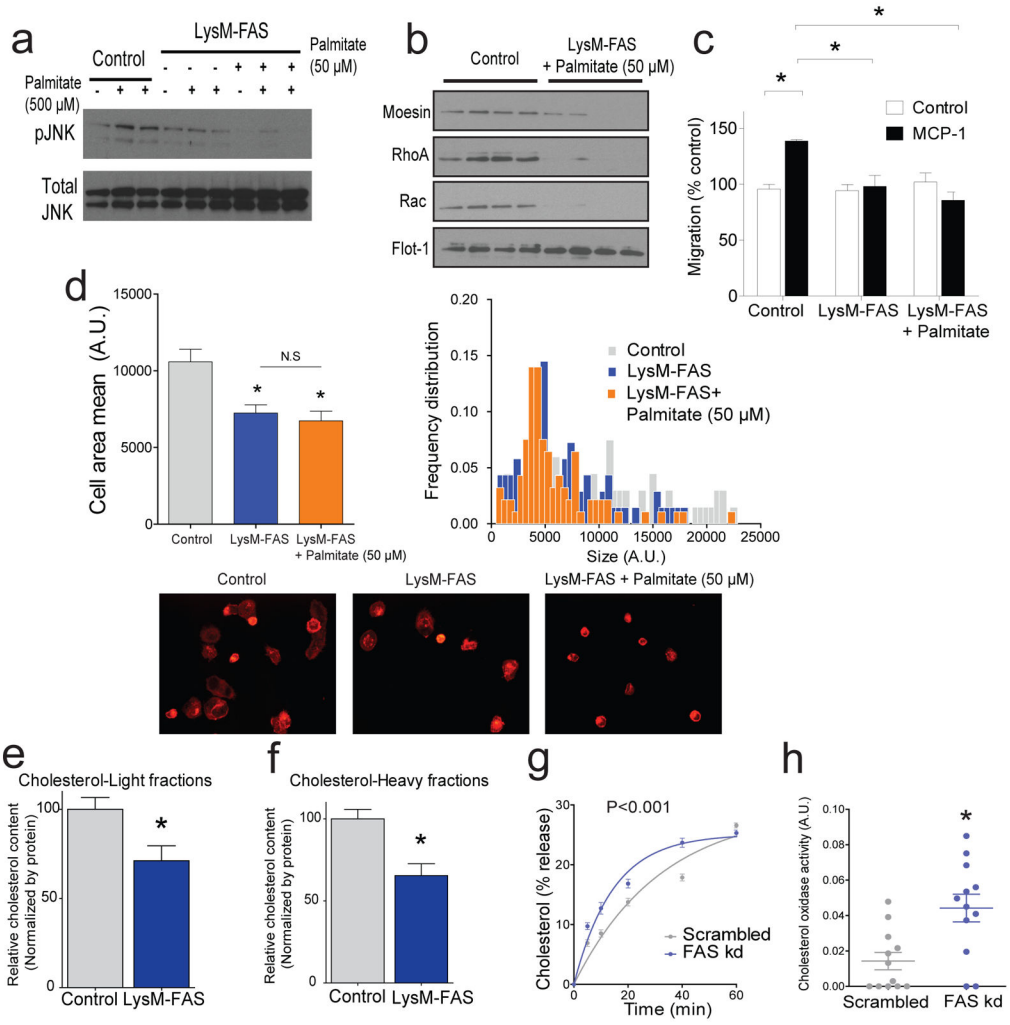

Extended Data Fig. 9. Chronic treatment with low dose palmitate does not rescue FASdependent macrophage defects, and cholesterol characterization

a. Phosphorylated JNK response to acute exposure to high dose palmitate (500 μM) in control macrophages and in FAS-knockout bone marrow-derived macrophages pretreated chronically with vehicle or 50 μM palmitate for 24 h. **b**. Western blotting of DRMs of LysM-FAS cells incubated with 50 μM palmitate for 24 h. **c**. MCP1-induced transwell migration assays of control and LysM-FAS cells demonstrating that palmitate incubation does not rescue the macrophage motility defect with FAS deficiency (n=4). **d**. Cell spreading assays for control macrophages, FAS-deficient macrophages, and FAS-deficient macrophages treated with 50 μM palmitate for 24 h. Cell area on the left, with frequency distribution of cell spreading on the right, and images of macrophage spreading on the bottom. n>100 for frequency distribution of cell spreading. **e, f**. Cholesterol content of fractions from LysM-FAS cells (n=4). **g**. Cholesterol release to methyl-β-cyclodextrin in control and FAS knockdown RAW cells (n=4). **h**. Cholesterol oxidase activity in control and FAS knockdown RAW cells (n=12). *P<0.05, except in **g** where P<0.001 by nonlinear curve fit comparison, symbols and error bars indicate mean ± s.e.m.

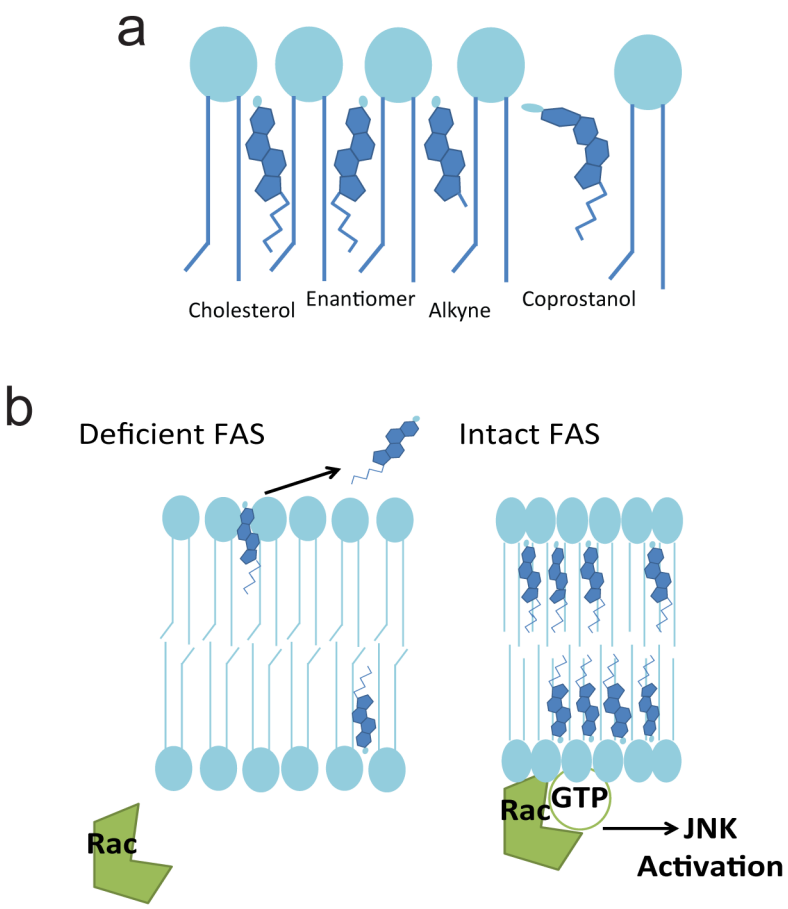

Extended Data Fig. 10. Schematic rendering of sterols in membranes

a. Generalized planar and nonplanar structures of sterols used to load macrophages. **b**. Diagram of FAS-dependent cholesterol retention at the plasma membrane leading to JNK activation. In the FAS-deficient state, the phospholipid environment is characterized by more unsaturated fatty acids while in the FAS-replete state, phospholipids are enriched in saturated fatty acids. For (**a**) and (**b**), phospholipids are depicted schematically and not intended to represent authentic unsaturated fatty acid structures.

Supplementary Material

Refer to Web version on PubMed Central for supplementary material.

Acknowledgments

This work was supported by NIH grants DK101392, DK076729, DK088083, DK20579, DK56341, RR00954, HL067773, and the Taylor Family Institute for Innovative Psychiatric Research. Steve Teitelbaum provided the constitutively active Rac construct, Tony Pryse performed confocal microscopy, Lihua Yang and Mark Miller assisted with imaging, and Laurel Mydock-McGrane prepared the cholesterol alkyne.

References

1. Olefsky JM, Glass CK. Macrophages, inflammation, and insulin resistance. Annu Rev Physiol. 2010; 72:219–246. [PubMed: 20148674]

2. Ferrante AW Jr. Macrophages, fat and the emergence of immunometabolism. J Clin Invest. 2013; 123:4992–4993. [PubMed: 24292661]
3. Carvalheira JB, Qiu Y, Chawla A. Blood spotlight on leukocytes and obesity. Blood. 2013; 122:3263–3267. [PubMed: 24065242]
4. Han MS, et al. JNK expression by macrophages promotes obesity-induced insulin resistance and inflammation. Science. 2013; 339:218–222. [PubMed: 23223452]
5. Lumeng CN, Saltiel AR. Inflammatory links between obesity and metabolic disease. J Clin Invest. 2011; 121:2111–2117. [PubMed: 21633179]
6. Koberlin MS, et al. A conserved circular network of coregulated lipids modulates innate immune responses. Cell. 2015; 162:170–183. [PubMed: 26095250]
7. Foster LJ, De Hoog CL, Mann M. Unbiased quantitative proteomics of lipid rafts reveals high specificity for signaling factors. Proc Natl Acad Sci U S A. 2003; 100:5813–5818. [PubMed: 12724530]
8. Yamashita T, et al. Enhanced insulin sensitivity in mice lacking ganglioside GM3. Proc Natl Acad Sci U S A. 2003; 100:3445–3449. [PubMed: 12629211]
9. Holzer RG, et al. Saturated fatty acids induce c-Src clustering within membrane subdomains, leading to JNK activation. Cell. 2011; 147:173–184. [PubMed: 21962514]
10. Zhou Y, et al. Membrane potential modulates plasma membrane phospholipid dynamics and K-Ras signaling. Science. 2015; 349:873–876. [PubMed: 26293964]
11. Maier T, Leibundgut M, Ban N. The crystal structure of a mammalian fatty acid synthase. Science. 2008; 321:1315–1322. [PubMed: 18772430]
12. Wei X, et al. De novo lipogenesis maintains vascular homeostasis through endothelial nitric-oxide synthase (eNOS) palmitoylation. J Biol Chem. 2011; 286:2933–2945. [PubMed: 21098489]
13. Geiger T, Cox J, Ostasiewicz P, Wisniewski JR, Mann M. Super-SILAC mix for quantitative proteomics of human tumor tissue. Nat Methods. 2010; 7:383–385. [PubMed: 20364148]
14. Simons K, Gerl MJ. Revitalizing membrane rafts: new tools and insights. Nat Rev Mol Cell Biol. 2010; 11:688–699. [PubMed: 20861879]
15. Gowrishankar K, et al. Active remodeling of cortical actin regulates spatiotemporal organization of cell surface molecules. Cell. 2012; 149:1353–1367. [PubMed: 22682254]
16. Lingwood D, Simons K. Lipid rafts as a membrane-organizing principle. Science. 2010; 327:46–50. [PubMed: 20044567]
17. Prag S, et al. Activated ezrin promotes cell migration through recruitment of the GEF Dbl to lipid rafts and preferential downstream activation of Cdc42. Mol Biol Cell. 2007; 18:2935–2948. [PubMed: 17538024]
18. Palazzo AF, Eng CH, Schlaepfer DD, Marcantonio EE, Gundersen GG. Localized stabilization of microtubules by integrin- and FAK-facilitated Rho signaling. Science. 2004; 303:836–839. [PubMed: 14764879]
19. Fessler MB, et al. Lipid rafts regulate lipopolysaccharide-induced activation of Cdc42 and inflammatory functions of the human neutrophil. J Biol Chem. 2004; 279:39989–39998. [PubMed: 15262974]
20. del Pozo MA, et al. Integrins regulate Rac targeting by internalization of membrane domains. Science. 2004; 303:839–842. [PubMed: 14764880]
21. Sezgin E, et al. Elucidating membrane structure and protein behavior using giant plasma membrane vesicles. Nat Protoc. 2012; 7:1042–1051. [PubMed: 22555243]
22. Levental I, Grzybek M, Simons K. Raft domains of variable properties and compositions in plasma membrane vesicles. Proc Natl Acad Sci U S A. 2011; 108:11411–11416. [PubMed: 21709267]
23. Lange Y, et al. Regulation of fibroblast mitochondrial 27-hydroxycholesterol production by active plasma membrane cholesterol. J Lipid Res. 2009; 50:1881–1888. [PubMed: 19401598]
24. Levental I, et al. Cholesterol-dependent phase separation in cell-derived giant plasma-membrane vesicles. Biochem J. 2009; 424:163–167. [PubMed: 19811449]
25. Westover EJ, Covey DF. The enantiomer of cholesterol. J Membr Biol. 2004; 202:61–72. [PubMed: 15702370]

26. York AG, et al. Limiting cholesterol biosynthetic flux spontaneously engages type I IFN signaling. Cell. 2015; 163:1716–1729. [PubMed: 26686653]
27. Wu M, et al. Antidiabetic and antisteatotic effects of the selective fatty acid synthase (FAS) inhibitor platensimycin in mouse models of diabetes. Proc Natl Acad Sci U S A. 2011; 108:5378–5383. [PubMed: 21389266]
28. Everts B, et al. TLR-driven early glycolytic reprogramming via the kinases TBK1-IKKepsilon supports the anabolic demands of dendritic cell activation. Nature Immunol. 2014; 15:323–332. [PubMed: 24562310]
29. Berod L, et al. De novo fatty acid synthesis controls the fate between regulatory T and T helper 17 cells. Nat Med. 2014; 20:1327–1333. [PubMed: 25282359]
30. Moon JS, et al. UCP2-induced fatty acid synthase promotes NLRP3 inflammasome activation during sepsis. J Clin Invest. 2015; 125:665–680. [PubMed: 25574840]
31. Schneider JG, et al. Macrophage fatty-acid synthase deficiency decreases diet-induced atherosclerosis. J Biol Chem. 2010; 285:23398–23409. [PubMed: 20479009]
32. Chakravarthy MV, et al. Identification of a physiologically relevant endogenous ligand for PPARalpha in liver. Cell. 2009; 138:476–488. [PubMed: 19646743]
33. Funai K, et al. Muscle lipogenesis balances insulin sensitivity and strength through calcium signaling. J Clin Invest. 2013; 123:1229–1240. [PubMed: 23376793]
34. Wei X, et al. Fatty acid synthase modulates intestinal barrier function through palmitoylation of mucin 2. Cell Host Microbe. 2012; 11:140–152. [PubMed: 22341463]
35. Monetti M, Nagaraj N, Sharma K, Mann M. Large-scale phosphosite quantification in tissues by a spike-in SILAC method. Nat Methods. 2011; 8:655–658. [PubMed: 21743459]
36. Wei X, Song H, Semenkovich CF. Insulin-regulated protein palmitoylation impacts endothelial cell function. Arterioscler Thromb Vasc Biol. 2014; 34:346–354. [PubMed: 24357059]
37. Levental KR, Levental I. Isolation of giant plasma membrane vesicles for evaluation of plasma membrane structure and protein partitioning. Methods Mol Biol. 2015; 1232:65–77. [PubMed: 25331128]
38. Owen DM, Rentero C, Magenau A, Abu-Siniyeh A, Gaus K. Quantitative imaging of membrane lipid order in cells and organisms. Nat Protoc. 2012; 7:24–35.
39. Lange Y, Ye J, Steck TL. How cholesterol homeostasis is regulated by plasma membrane cholesterol in excess of phospholipids. Proc Natl Acad Sci U S A. 2004; 101:11664–11667. [PubMed: 15289597]
40. Jiang X, et al. A sensitive and specific LC-MS/MS method for rapid diagnosis of Niemann-Pick C1 disease from human plasma. J Lipid Res. 2011; 52:1435–1445. [PubMed: 21518695]
41. Ciepla P, et al. New chemical probes targeting cholesterylation of Sonic Hedgehog in human cells and zebrafish. Chem Sci. 2014; 5:4249–4259. [PubMed: 25574372]

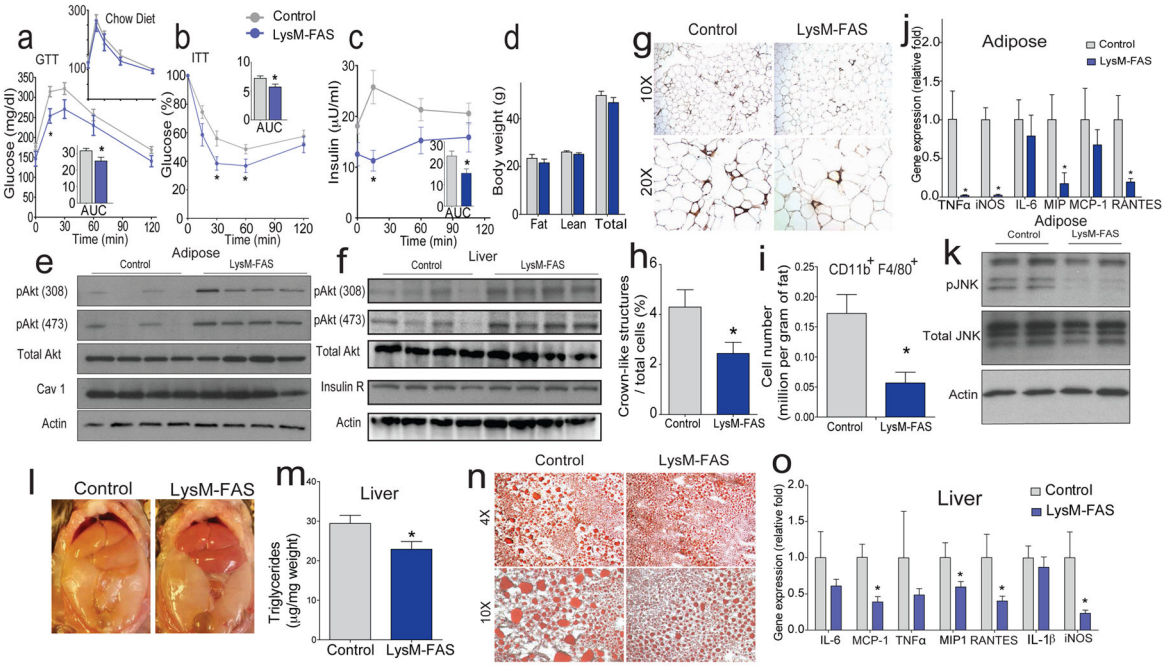

Fig. 1. Macrophage FAS ablation ameliorates diet-induced insulin resistance and inflammation in mice

a. Glucose tolerance test (GTT-upper inset on chow diet), (**b**) insulin tolerance test (ITT), and (**c**) glucose-stimulated insulin secretion in LysM-FAS mice fed HFD for 3 months (n=10 control and 7 LysM-FAS). AUC indicates area under the curve. **d.** Body composition for the mice of **a–c. e, f.** Insulin-stimulated Akt phosphorylation in adipose tissue (**e**) and liver (**f**) of control and LysM-FAS mice. **g.** Photomicrographs, crown-like structures (**h**), and macrophages (**i**) in visceral adipose tissue of HFD-fed mice (n=4 per group). **j.** Inflammatory gene expression (n=7 control and 6 LysM-FAS) and (**k**) JNK phosphorylation in adipose tissue of control and LysM-FAS mice. **l.** Gross appearance and (**m**) triglyceride content of liver from control (n=6) and LysM-FAS mice (n=8). **n.** Oil red O staining and (**o**) inflammatory gene expression in livers from control (n=6) and LysM-FAS mice (n=8). *P<0.05, symbols and error bars indicate mean ± s.e.m.

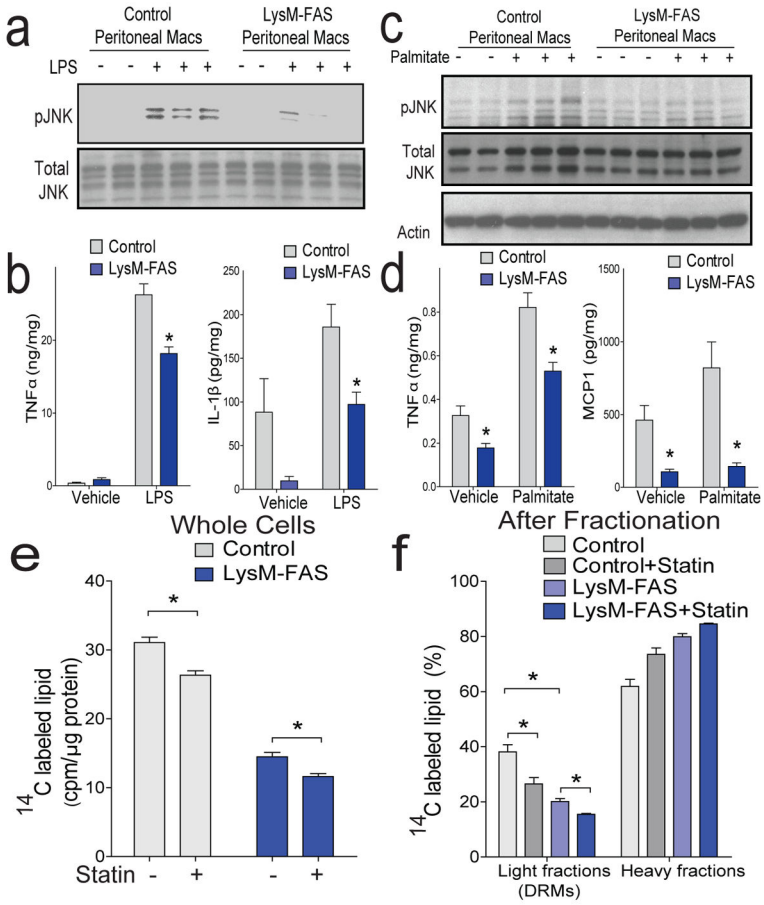

Fig. 2. Macrophage FAS deficiency attenuates cell autonomous inflammation and alters detergent-resistant microdomains (DRMs)

a, b. JNK phosphorylation (**a**) and cytokine stimulation (**b**) by LPS in peritoneal macrophages. **c, d.** JNK phosphorylation (**c**) cytokine stimulation (**d**) by palmitate in peritoneal macrophages. **e.** Radioactivity in whole cell lipid extracts from control and FAS-knockout macrophages in the absence or presence of simvastatin (10 μM, 24 h), and (**f**) percent radioactivity in lipid extracts from light or heavy fractions (n=4 per condition). ELISAs (**b** and **d**) were performed in triplicate for each isolation, and repeated three times using different mice. *P<0.05, symbols and error bars indicate mean ± s.e.m.

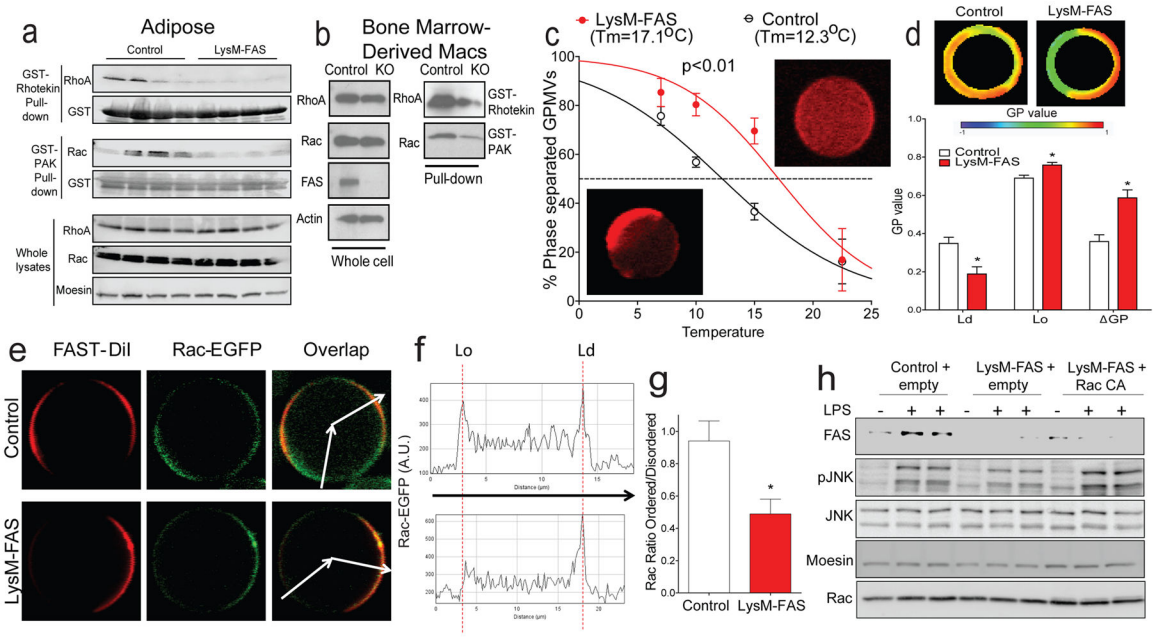

Fig. 3. FAS deficiency disrupts Rho GTPases and alters membrane order

a. Western blotting of activated RhoA (top panel), activated Rac (middle panel), and total RhoA and Rac (bottom panel) in adipose tissue of control and LysM-FAS mice. **b.** Total (left), or activated (right) Rho GTPases in control or FAS-knockout bone marrow-derived macrophages. **c.** Giant plasma membrane vesicles (GPMVs) prepared from bone marrow-derived macrophages were labeled with the liquid disordered fluorescent dye FAST-DiI and cooled in a step-wise manner followed by scoring vesicles for phase separation by confocal microscopy. Insets show phase-separated (lower left) and non-separated (upper right) vesicles. **d.** General polarization values were determined using the dye Di-4-ANEPPDHQ. Ld indicates liquid disordered and Lo indicates liquid ordered domains. **e.** Cells were transduced with a Rac-EGFP construct followed by preparation of GPMVs and staining with the Ld dye FAST-DiI. Lo and Ld domains for quantification are indicated by arrows. **f.** ImageJ scan of Lo and Ld domains. **g.** Rac partitioning in ordered vs. disordered domains. **h.** Cells were transduced with a constitutively active Rac (Rac CA) followed by determination of JNK phosphorylation with LPS stimulation. Imaging analyses (**c–e**) were performed in >40 vesicles per condition in isolated cells from 3 different mouse pairs. Data in (**c**) represent pooled numbers, and data in (**d–g**) are representative experiments with 5–6 vesicles per group. *P<0.05, symbols and error bars indicate mean ± s.e.m.

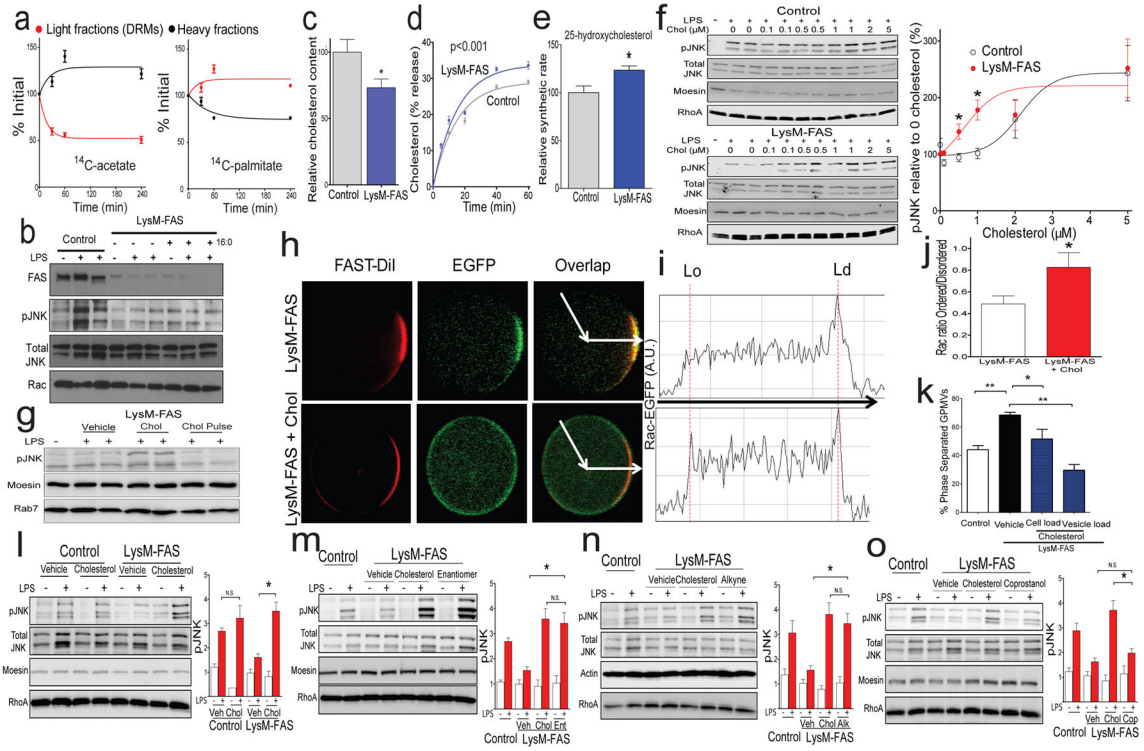

Fig. 4. Exogenous palmitate does not rescue inflammation, but exogenous cholesterol restores JNK signaling, membrane order, and Rho GTPase membrane distribution

a. Pulse-chase turnover of ^{14}C-acetate (left) or ^{14}C-palmitate-labeled lipids (right) in DRMs vs. heavy fractions (n=4). **b.** Chronic incubation with 50 μM palmitate does not restore JNK responsiveness. **c.** Cholesterol content normalized by protein (n=8), (**d**) cholesterol release to methyl-β-cyclodextrin (n=4), and (**e**) oxysterol synthesis in control and FAS-deficient cells (n=5). **f.** Control and LysM-FAS macrophages were loaded with 0–5 μM cholesterol using methyl-β-cyclodextrin followed by stimulation with LPS. Representative blots are shown on the left and quantification on the right (n=5). **g.** FAS-deficient macrophages were loaded with 1 μM cholesterol (Chol) followed immediately by LPS stimulation or by 2 h before LPS stimulation (Chol Pulse). **h.** Cells expressing Rac-EGFP were subjected to vehicle or cholesterol loading followed by preparation of GPMVs and staining with the Ld dye FAST-DiI. Lo and Ld domains for quantification are indicated by arrows. **i.** ImageJ scan of Lo and Ld domains. **j.** Rac partitioning in ordered vs. disordered domains with cholesterol loading. **k.** Phase separation in cholesterol-treated FAS deficient GPMVs. **l–o.** Bone marrow-derived macrophages from control and FAS-deficient mice were loaded with vehicle or 1 μM sterol followed by LPS stimulation and analysis of JNK phosphorylation. Loading was performed with natural cholesterol (**l**), enantiomeric cholesterol (**m**), the alkyne (3β)-26,27-dinorcholest-5-en-24-yn-3-ol (**n**), and the nonplanar sterol coprostanol (**o**). Representative blots are shown with quantification (n=4) to the right of each set of blots. Imaging analyses (**h–k**) were performed in isolated cells from 3 different experiments. Data in (**j**) are from a representative experiment with 9–10 vesicles per group, and data in (**k**) represent pooled

numbers. *P<0.05, **P<0.01, except for **d** where P<0.001 by nonlinear curve fit comparison, symbols and error bars indicate mean ± s.e.m.